ISPRS Journal of Photogrammetry and Remote Sensing 166 (2020) 268–277

Contents lists available at ScienceDirect

ISPRS Journal of Photogrammetry and Remote Sensing

journal homepage: www.elsevier.com/locate/isprsjprs

Fully automatic smartphone-based photogrammetric 3D modelling of infant's heads for cranial deformation analysis

Inés Barbero-García*, José Luis Lerma, Gaspar Mora-Navarro

Department of Cartographic Engineering, Geodesy and Photogrammetry, Universitat Politècnica de València, Camino de Vera, s/n, Building 7i, 46022 Valencia, Spain

ARTICLE INFO

Keywords:
3D modelling
Medicine
Plagiocephaly
Smartphone
Photogrammetry

ABSTRACT

Image-based and range-based solutions can be used for the acquisition of valuable data in medicine. However, most of these methods are not valid for non-static patients. Cranial deformation is a problem with high prevalence among infants and image-based solutions can be used to assess the degree of deformation and monitor the evolution of patients. However, it is required to deal with infants normal movement during the assessment in order to avoid sedation. Some high-end multiple-sensor image-based solutions allow the achievement of accurate 3D data for medical applications under unpredicted dynamic conditions in consultation. In this paper, a novel, single photogrammetric smartphone-based solution for cranial deformation assessment is presented. A coded cap is placed on the infant's head and a guided smartphone app is used by the user to acquire the information, that is later processed on a server to obtain the 3D model. The smartphone app is designed to guide users with no knowledge of photogrammetry, computer vision or 3D modelling. The processing is fully automatic offline. The photogrammetric tool is also non-invasive, reacting well with quick and sudden infant's movements. Therefore, it does not require sedation. This paper tackles the accuracy and repeatability analysis tested both for a single user (intrauser) and multiple non-expert user (interuser) on 3D printed head models. The results allow us to confirm an accuracy below 1.5 mm, which makes the system suitable for clinical practice by medical staff. The basic automatically-derived anthropometric linear magnitudes are also tested obtaining a mean variability of 0.6 ± 0.6 mm for the longitudinal and transversal distances and 1.4 ± 1.3 mm for the maximum perimeter.

1. Introduction

Image-based and range-based technologies can be useful for a wide range of medical applications and are assumed to have great potential. Photogrammetric techniques have been introduced as an important medical imaging tool, providing higher accuracy and improving existing techniques (Mitchell and Newton, 2002; Patias, 2002). Image-based solutions have also proved to be useful for external body documentation and easy to use for static targets (Urbanová et al., 2015). Image-based and range-based technologies can be used for purposes such as prosthetics design (Grazioso et al., 2019), surgery planning (Kournoutas et al., 2019), deformation assessment (Jodeh et al., 2018) or obtainment of anthropometric measurements (Heymsfield et al., 2018), among others.

However, the inclusion of image-based and range-based solutions in the daily routine of medical clinics and hospitals still poses a challenge mainly due to expensive medical devices and lack of portability (Nahles et al., 2018; Siegenthaler, 2015; Sirazitdinova and Deserno, 2017).

Cranial deformation is a problem with high prevalence among infants (Peitsch et al., 2004). It has different causes, from positional ones to early closure of cranial sutures. The most common type of deformation is positional plagiocephaly, that affects, at different degrees, approximately 40% of infants (Ballardini et al., 2018; Khormi et al., 2020). The prevalence of positional plagiocephaly increased dramatically in the 1990s as a consequence of the "Back to Sleep Campaign" of the American Association of Pediatrics, which recommended maintaining infants on their backs when sleeping in order to prevent the sudden infant death syndrome (Kattwinkel et al., 2000).

Deformational plagiocephaly is usually considered to cause esthetical problems only. However, some authors have stated some correlation between positional deformations and developmental delays (Collett et al., 2019; Martiniuk et al., 2017). For this reason, the accurate detection and evaluation of deformation in the early stages is considered extremely useful. Other types of deformations such as craniosynostosis, caused by sutures of the cranial vault closing prematurely, are more complex to treat and usually require surgery. Craniosynostosis can involve esthetical problems but also visual deficit, hydrocephalus and increased cranial pressure. The early detection of

* Corresponding author.
E-mail address: inbargar@topo.upv.es (I. Barbero-García).

https://doi.org/10.1016/j.isprsjprs.2020.06.013
Received 14 April 2020; Received in revised form 4 June 2020; Accepted 16 June 2020

this pathology is important to assure the possible outcomes (Ursitti et al., 2011). Assessment of the surgical outcome is also a requirement where photogrammetry can play an important role.

Different approaches are followed to evaluate cranial deformation in infants. The most simple approach is visual assessment, usually following the indications given by Argenta (2004). The most commonly used devices in consultation are callipers and disposable paper measuring tapes (Siegenthaler, 2015; Wilbrand et al., 2011). These devices require hand measurements, are inexpensive, non-invasive and follow normative guidelines (Farkas, 1994). However, authors differ in the accuracy and reliability of the results of these subjective manual measurements, some of them quantifying an interuser accuracy of 2 mm (Mortenson and Steinbok, 2006; Wilbrand et al., 2011). The disadvantages of the manual measurements are the difficulties for getting valuable results after training and the time required to perform repeated measurements. Moreover, the obtained information, consisting in a in a small number of measurements, is very limited in comparison with a 3D model (Wong et al., 2008).

The gold standards in radiologic medical imaging are Computed Tomography (CT) and nuclear Magnetic Resonance Imaging (MRI). These gold standards for diagnostic and therapeutic purposes provide the most accurate and complete information (not only out, but most importantly, inside the head through cross-sectional images) and are often necessary when infant's head craniosynostosis is not discarded. However, these techniques are costly and invasive as sedation of the patient is usually required. For these reasons, routine CT and MRI are not common in clinical routine (Argenta, 2004). Moreover, to evaluate purely aesthetical outcomes CT and MRI are limited by the lying position of the infants. This position can alter the soft tissue in some areas of the head due to gravity and pressure of the support area (Barbero-García et al., 2019; Caple et al., 2016; Munn and Stephan, 2018). The alteration in the head's shape can be easily observed once the 3D models are reconstructed.

Multi-scanner and/or multicamera setups provide complete information of the head's shape with high accuracy (Lübbers et al., 2010). These high-end image-based and/or range-based devices are non-invasive and nowadays are adapted to perform the data acquisition even with uncollaborative and moving infants. These devices deliver also accurate 3D models of the external head's shape and are used for different cranial deformation studies, including diagnosis (Meulstee et al., 2017), assessment of surgical outcomes (de Jong et al., 2017), evaluation the effects of orthotic helmets (Dörhage et al., 2018) or to define normal head parameters (Hsu et al., 2019). Despite its advantages, these high-end image-based and/or range-based devices are not integrated as part of the clinical practice due to their high costs (Khormi et al., 2020).

For the accurate evaluation of cranial deformation, an accurate 3D model of the patient's head (infants ranging usually from 1 to 24 months old) must be delivered during a normal consultation, in a way that the medical staff can make right diagnosis and decisions. In the case of cranial deformation analysis, most limitations are given by the movement of the infants (Barbero-García et al., 2017). In order to create a useful and low-cost medical device, it is vital to deal with the movement and produce highly accurate 3D models in real clinical conditions.

The use of photogrammetric devices by non-experts, such as medical staff, requires a high degree of automation and reliability (Nocerino et al., 2017). It is also important to extract the information in short periods as the consultation time is, in most cases, very limited. Besides, the metric solutions have to be robust and reliable enough to satisfy challenging health demands.

The automation possibilities are different regarding the requirements and conditions of every particular medical application. The use of coded markers, under different setup geometries and the required number of images to extract useful infant's head 3D models have been explored by the authors (Barbero-García et al., 2018). The accuracy of manually-driven 3D models has also been tested by the authors in comparison with the present gold standards, CT and MRI (Barbero-García et al., 2019). However, a fully automatic methodology for the extraction of the 3D models has not been presented.

Automatic camera pose estimation and calibration are usually carried out using automatically detected keypoints. The obtainment of these keypoints is commonly carried out using algorithms such as SIFT (Lowe, 1999) or SURF (Bay et al., 2007), or more novel robust approaches based on ASIFT (Wang et al., 2018). Obtaining keypoints is time-consuming when dealing with large datasets. For moving objects, some type of masking is required to assure that the keypoints are located in the object and not in the background.

The target-based approach is an alternative to the keypoints approach for camera pose estimation. It is especially useful for low-texture areas where not enough keypoints can be identified (Muñoz-Salinas et al., 2018). The target-based approach is not always an option as the placement of the targets is not possible in many situations when the object to be modelled cannot be altered. For this particular application, a cap is placed on the patient's head and the texture of the model does not add any useful information. For this reason, the placement of markers is not an issue. Moreover, with this approach, the movement of the background will not be a problem, as all markers are placed on the cap.

The targets chosen for this study are ArUco markers. ArUco markers include a black frame that allows quick detection and binary code for identification. For every marker, four points (corners) can be automatically identified with subpixel accuracy (Garrido-Jurado et al., 2016; Romero-Ramirez et al., 2018). This type of markers has been used for calibration of low-cost cameras (Da Silva et al., 2014).

In this study, a novel and fully automatic solution for the creation of the infant's head 3D models is presented. The solution consists of a mobile app, a coded cap and processing software. First, the cap is placed in the infant's head. Then a doctor or any user would use the mobile app to get the necessary data for the creation of the 3D models. The whole process is guided so the user is not required to have any knowledge of photogrammetry. Once all the required data is collected, it is sent to a server where it is processed to obtain the final 3D model, which is presented to the doctor in several minutes.

2. Materials and methods

2.1. Automatic PhotoMeDAS tool

The PhotoMeDAS (Photogrammetric Medical Deformation Assessment Solutions) patent-pending tool is composed of coded cap, coded stickers, mobile app and processing software. The mobile application is used together with the cap and stickers to carry out the data acquisition. The software, located in a server, processes the data and creates a 3D model. It also obtains some head shape information and deformation parameters, which are available to the user through a webpage service (Fig. 1).

2.1.1. Coded cap

The cap is made of an elastic material on which coded ArUco markers have been added. Each cap contains a total of 131 markers, the material of the markers is not elastic to assure their size is constant and can be used to scale the model (Fig. 2).

Together with the cap, three stickers are provided. The stickers are similar to the markers present on the cap. The medical staff carrying out the image acquisition are asked to place one of them between the eyes and the others on the left-hand side and right-hand side pre-auricular points. The identification of these points will be used for the registration of the models (monitoring) over time (Fig. 2).

The mobile app allows data acquisition by users without understanding of the photogrammetric principles. The following criteria has been implemented to assure that any user can carry out a successful

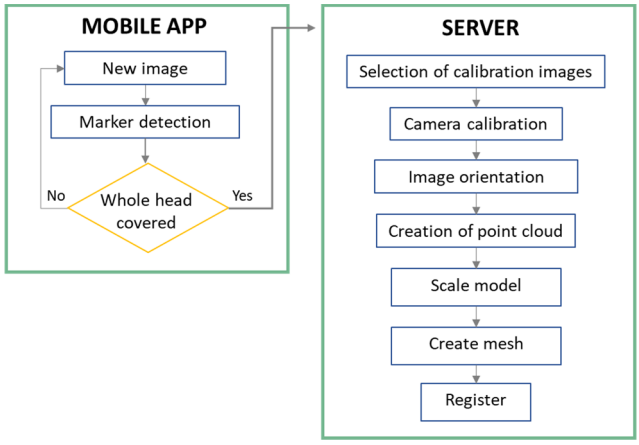

Fig. 1. Implemented photogrammetric workflow.

data acquisition: (i) the detected markers are highlighted in the image; (ii) the correctly registered areas are shown; and (iii) a progress bar shows the progress percentage.

Each frame is checked for valuable information by the app. Firstly, it must have more than 7 markers (a lower number does not assure successful orientation). Moreover, the sets of markers in the image are evaluated to assure there is information in the image that is not already registered (a previous frame with the same set of markers would discard the current image). In case the image is selected, the coordinates of the markers are saved to a file. For each marker, the coordinates of the four corners are stored. At the same time, the app is updated to show the new registered areas on the screen.

This particular approach has been designed to deal with the movement of the infant. If the patient is moving it hampers the image acquisition and no markers are detected, therefore the frames are ignored. As soon as the patient is still enough, even for a short period, the application will record the information.

More than 200 images covering the totality of the model are required to assure a good orientation (Barbero-García et al., 2018). Once the required number of images is registered and the whole head is correctly covered, the app will automatically send the data for processing.

2.1.2. Model creation

The model creation is carried out on a server. The server runs a Django (Django Software Foundation, Lawrence, KS) WSGI (Web Server Gateway Interface) application. When a model data is received the application stores the file and inserts the model metadata into a PostgreSQL database. Then, it runs the model calculation algorithm as a Celery Distributed Task Queue process and informs the user. Celery remains calculating the model as a background process in the server. The server can process several models at once. If there are many models to calculate at a time, they are put in a queue. When Celery finishes the calculation, an alert is sent to the user and the final model is made available on the webpage (Fig. 3).

The modelling calculation software was created using a combination of open-source software and ad-hoc developed software. First of all, the received data is checked. The frames are evaluated in order to remove redundancy from the recorded data. This step improves the selection carried out during the data acquisition. Secondly, the frames for calibration are selected. The required frames will cover the top of the cap, giving the best possible geometry for calibration.

The software MicMac (Pierrot Deseilligny and Clery, 2012), and, specifically, the tools Tapas and AperiCloud, are used to obtain the 3D point cloud. MicMac tool Tapas is launched to carry out an on-the-job bundle adjustment camera calibration. For this camera calibration step, a reduced set of frames is selected, and if the results achieved are correct, the interior orientation parameters are extended to all the frames. Once the frames are oriented, the point cloud is then obtained using AperiCloud (Fig. 4a, b). In case the bundle adjustment results are not correct, another bundle adjustment process is carried out again for the whole set of frames.

The resulting point cloud consists of up to 536 points. It is scaled using the markers size and the point normals are computed automatically using MeshLab 1.3.3 (Cignoni et al., 2008). The mesh is also created automatically using the Ball Pivoting Algorithm (Bernardini et al., 1999) (see Fig. 4c, d).

The last step is the registration of the 3D model to a set head's local coordinate system (Fig. 5). The three points identified with stickers are used for the 3D registration among corresponding models. The y-axis will be given by the preauricular points while the frontal point and the centre between the ears define the x-axis.

The whole process presented in this section has been integrated using an in-house Python script and it is fully automatic. The script is automatically computed every time a data file is sent to the server.

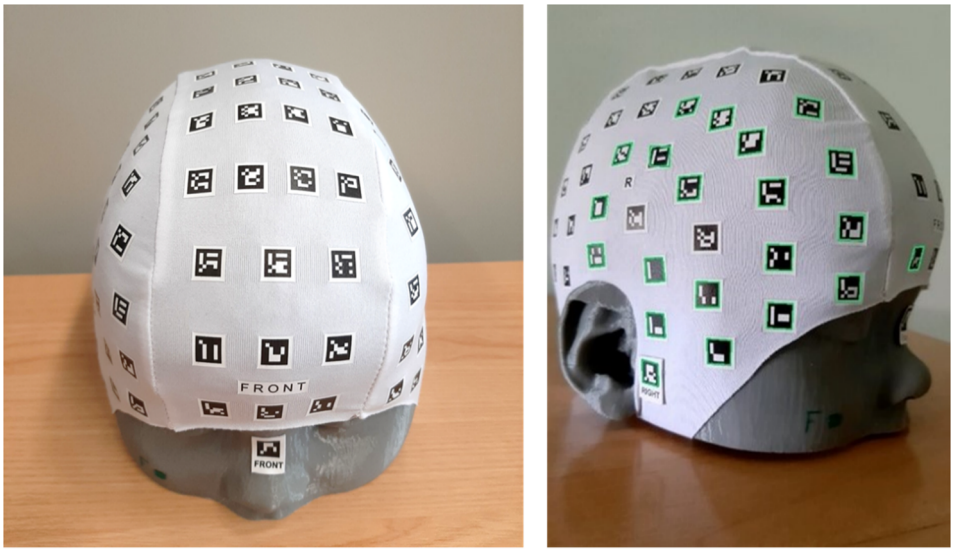

Fig. 2. (a) Coded cap and stickers; (b) view of the cap on the app.

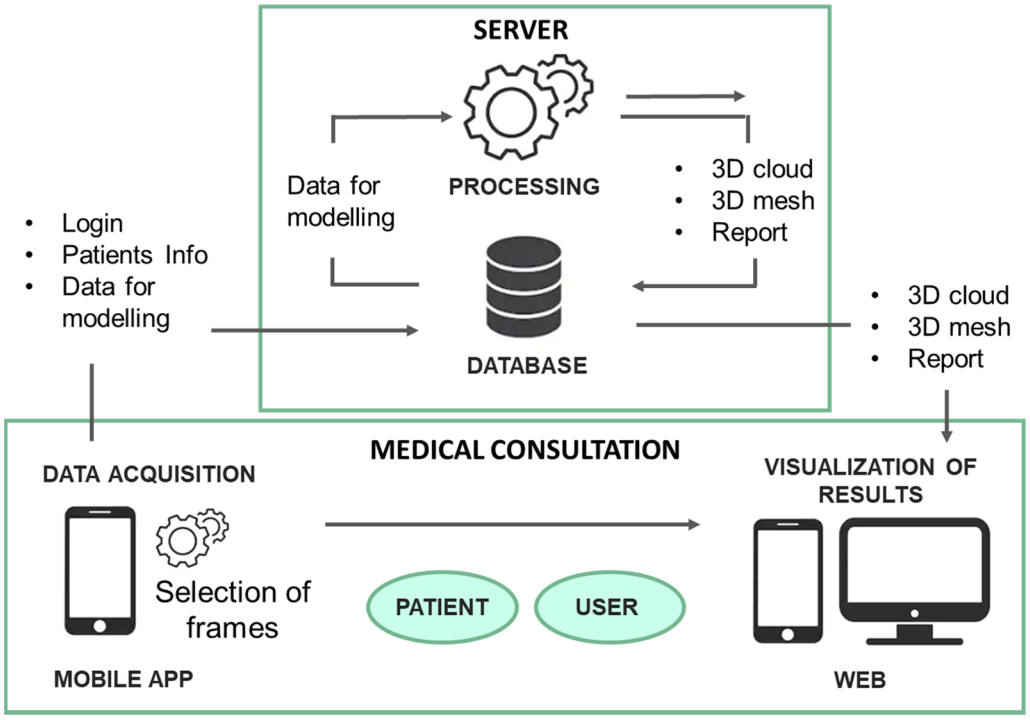

Fig. 3. PhotoMeDAS diagram.

2.1.3. Automatically-derived anthropometric linear magnitudes

Virtual 3D models by themselves have a reduced utility for doctors. It is necessary to obtain objective parameters and indexes that give direct information on the type and degree of deformation. To obtain the automatically-derived anthropometric linear magnitudes models are registered as presented in Section 2.1.2. In this study, three basic anthropometric linear magnitudes to yield indexes are obtained for each model, maximum perimeter, maximum longitudinal distance and maximum transversal distances. The values are obtained by iterative computation in a given direction and allowing small variations to obtain the longest values.

The perimeter is computed for a plane at different heights along the z-axis and different rotations in the y-axis (Phi angle), but without rotations in the x-axis or z-axis (Omega and Kappa angles) as this orientation is given by the preauricular points. The maximum longitudinal distance is computed as the maximum distance between a point

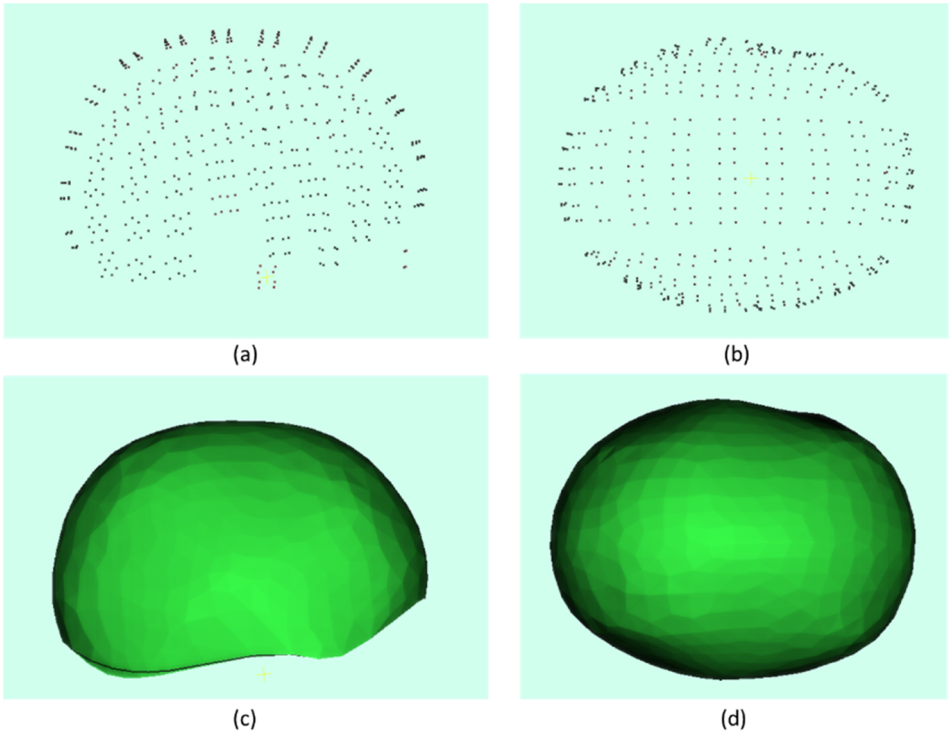

Fig. 4. 3D point cloud of the markers (a, side view; b, top view) and mesh (c, side view; d, top view).

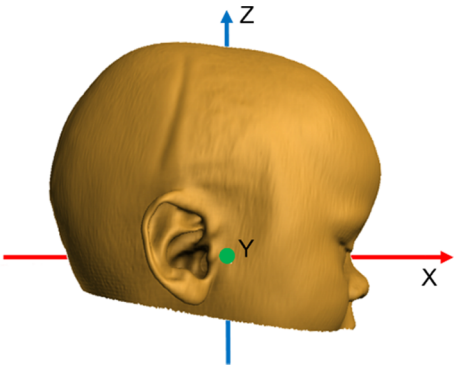

Fig. 5. The head's local coordinate system.

in y = 0 and located in the front of the head (front centred but at different heights) and points located in the back part of the head with same y coordinate, small rotations (maintaining the front point fixed) were allowed to deal with registration inaccuracies. The maximum transversal distance is computed along y-axis, no rotations are allowed.

2.2. Validation methodology

Five models of real infants' heads are obtained from Computed Tomography or Magnetic Resonance images. The 3D models are reconstructed using InVesalius (Centro de Tecnologia da Informação Renato Archer (CTI), Brazil). An example of the external output data is displayed in Fig. 5. The models obtained with the gold standards imaging devices are later 3D printed using a BQ printer. Those five models will be referred to as targets (Fig. 6). The 3D printed head has definitely an error but it can be considered negligible in comparison with the minor fitting imperfections covered by the coded cap.

The targets represent different types of cranial shape and deformation in infant's heads: (1) Scaphocephaly, long and narrow head caused by early fusion of sagittal suture; (2) Plagiocephaly, asymmetric distortion with a flattened area; (3) Complex deformation due to intrauterine constraint; (4) Trigonocephaly, early fusion of the metopic suture causing a triangular shape of the forehead; and (5) Normal shape considered without deformation (Fig. 6).

Intrauser and interuser repeatability and accuracy tests are carried out for each model. For the intrauser analysis, the same person carries out 25 data acquisition per targets. For the interuser tests, 25 different people acquires the data for each target. In total 250 models (125 intrauser and 125 interuser) are created, 50 for each target. For every data acquisition, the cap and stickers are placed by the user. A short introduction (less than one minute) on the tool is given to the user, however, no further training is provided.

2.2.1. Comparison between 3D models

The accuracy is measured by comparing every model with the digital version of the model used for 3D printing, considered as the ground truth. The repeatability is evaluated by comparing each pair of photogrammetric 3D models. Iterative Closest Point (ICP) (Besl and McKay, 1992; Goebbels et al., 2019; Heymsfield et al., 2018) algorithm is computed for each pair of models in order to improve the registration. For each pair of models, the distance is later computed along the ray from the centre of the model for each point in a sphere (Fig. 7). This methodology is chosen as it is proven to yield less noisy results than distances computed along the normals; besides, the provided measurements are well-distributed across the infant's head, as proposed by de Jong et al. (2017).

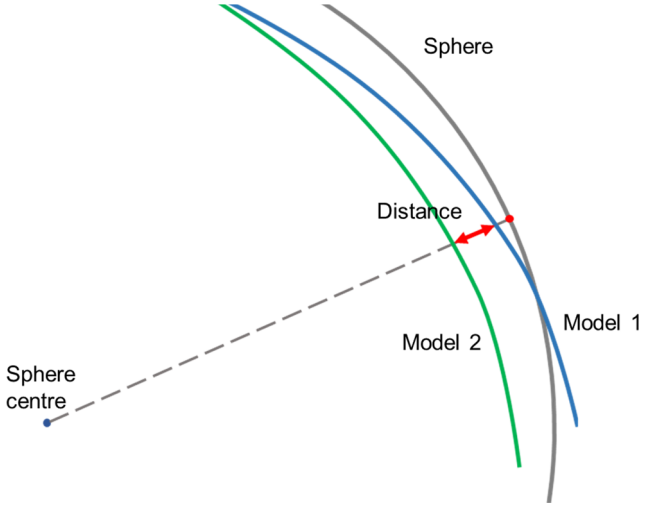

Fig. 7. Diagram displaying the distance computed between 3D models.

3. Results

The differences between target models are presented in Fig. 8. All tests resulted in a sum below 1 mm for mean plus standard deviation. The absolute differences are slightly larger for the interuser tests in comparison to those carried out by a single user (intrauser). Besides, the accuracy results are slightly worse (larger values) than the repeatability results. The mean accuracy is 0.5 ± 0.4 mm, and the repeatability differences are 0.3 ± 0.3 mm.

Ideally, there should be no significant differences in the results for different tests (comparing intrauser-interuser and repeatability-accuracy). A Student *t*-test was used to compare the results (understood as distances between models) for different tests. The 95% confidence interval for the difference in means between repeatability and accuracy results is 0.169–0.173 mm. For the comparison between intrauser and interuser tests, *t*-test 95% confidence interval of the difference in mean of the results is 0.073–0.74 mm. Therefore, for both comparisons (intrauser-interuser and repeatability-accuracy) it can be stated that the difference in the results is below 1 mm.

Absolute differences per model are presented in Fig. 9. No important differences are present for Target 1–4. Slightly worse results are presented for Target 5.

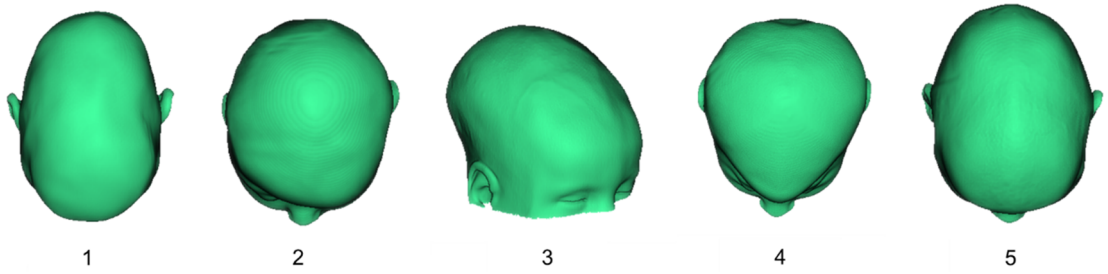

Fig. 6. Targets.

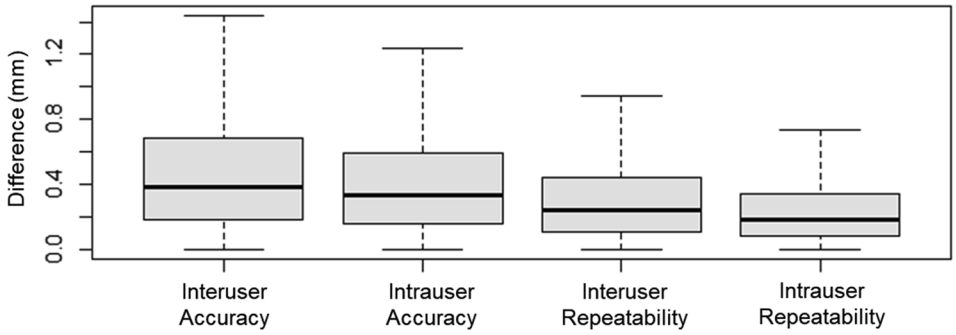

Fig. 8. Box plots of absolute differences between models for each test.

As it could be expected due to the effect of the cap, all photogrammetric 3D models showed an overestimation of measurements compared to the ground truth targets. Therefore, this resulted in positive distances (Fig. 10).

The mean and standard deviation for each comparison are shown in Fig. 11. Some models present an error considerable higher than the average, but in every case, the sum of mean and standard deviation is always below 2 mm.

Data acquisition and calculation time were registered for each created model. For the models created by a single user familiar with the methodology, the acquisition time was 1.1 ± 0.17 min. For various users, the acquisition time was higher: 1.5 ± 0.6 min. The calculation time was 2.5 ± 0.6 min for the expert user and 2.7 ± 0.9 min for different users, many of them with no previous knowledge of the tool.

For the five targets, the variability of the three most important anthropometric linear magnitudes is presented: perimeter, longitudinal and transversal distances. A Student's *t*-test was also performed to evaluate the significance of the difference in mean between intrauser and interuser tests. A second *t*-test was performed to test the hypothesis of the differences in means being greater than 1 mm. Table 1 summarises the results achieved from the automatically-derived anthropometric linear magnitudes for each target.

The measurement of the perimeter yields the lowest reliability with a difference with the mean of 1.4 ± 1.3 mm. For the maximum distances, the differences are 0.7 ± 0.6 mm for the longitudinal distance and 0.5 ± 0.5 mm for the transversal distances.

Student's *t*-test is performed to evaluate the differences in the means between intrauser and interuser measurements. A P-value below 0.05 is interpreted as a significant difference between the means. According to this threshold, some anthropometric magnitudes (all for Target 3, the perimeter for Target 4 and the perimeter and the longitudinal distance for Target 5), show significant differences for intrauser and interuser tests. Although significant, the difference values are low, and only for the Target 3 perimeter can be stated that the mean difference between interuser and Intrauser value is significantly greater than 1 mm.

4. Discussion

In this section, we discuss the advantages and limitations of the created photogrammetric tool and its applicability for cranial deformation assessment. The results are evaluated in two different ways: the accuracy achieved in the targets (3D models) and the accuracy of the automatically-derived anthropometric linear magnitudes. The factors that limit the accuracy of the results are also studied, and future lines of research for the improvement of the solution are presented.

4.1. The automatic tool

A fully automatic tool for the creation of head 3D models has been presented. The tool is adapted to the necessities of cranial deformation assessment in infants. In particular, it overcomes limitations, such as the almost constant movement of the infants during the data acquisition, it requires very low investment (from the user side only a smartphone is required) and does not require the user to have any knowledge of photogrammetry, being applicable to the standard clinical routine.

The designed methodology, based on markers, has very low requirements of data storage and transference. This is especially useful as the data requires to be sent to the servers during the consultation. Not all hospitals and clinical centres have high-speed networks.

The average acquisition and processing time was 3.9 min, while the longest time was 7.6 min. This processing time means a huge improvement in comparison with the manual photogrammetric process, that can require hours of expert work to achieve an accurate model (Barbero-García et al., 2017). This processing workflow makes the tool viable in normal clinical practice. One advantage is that once the user gets familiar with the photogrammetric tool, the processing time goes down, as reflected with the different between intrauser and interuser tests.

4.2. 3D models

A final accuracy of 1.5 mm was achieved. The purpose of the

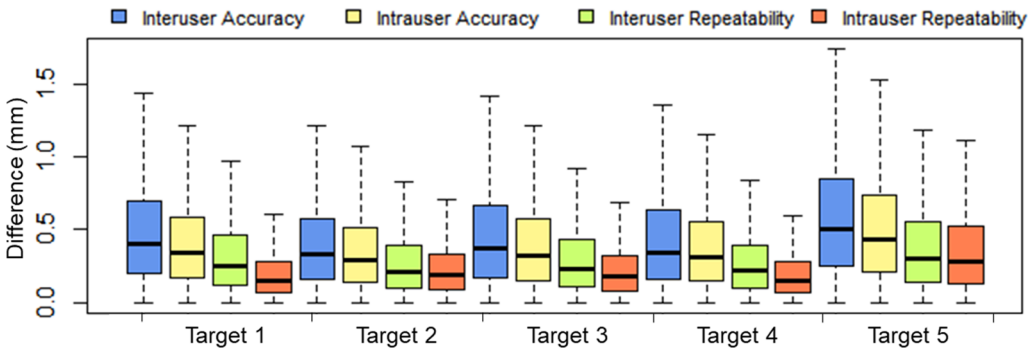

Fig. 9. Box plot of absolute differences between models for each test and model.

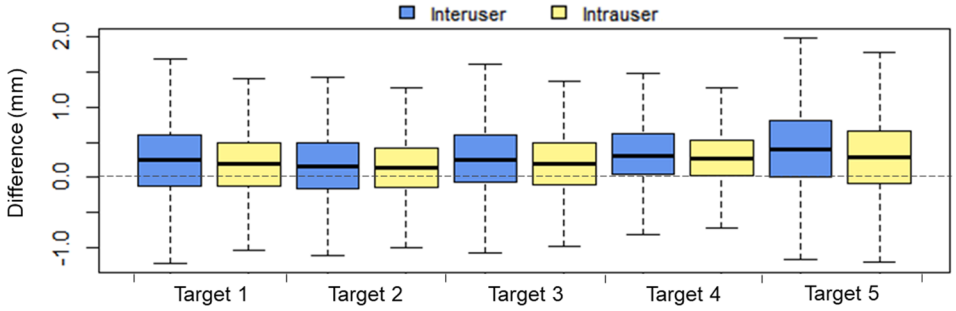

Fig. 10. Box plot of signed differences for the accuracy tests.

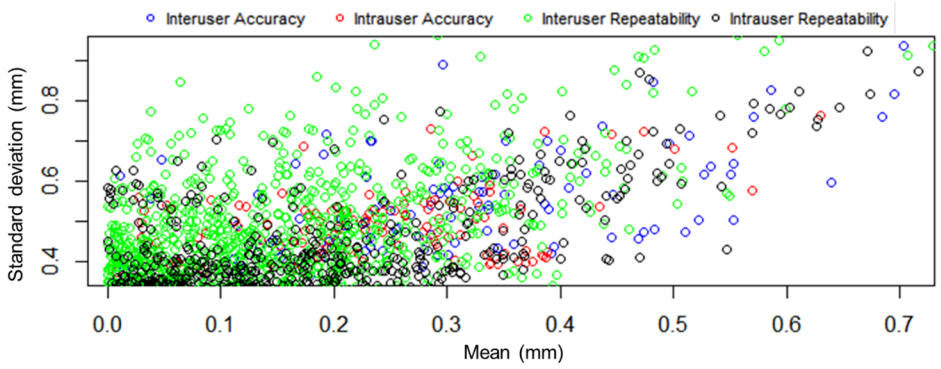

Fig. 11. Mean and standard deviation for each created model.

research project was not to deliver the highest possible accuracy but reliable measurements for doctors with real-life available devices, i.e. smartphones. From a photogrammetric standpoint, this result could be considered somehow above the required standards for cranial deformation assessment. However, medical staff suggest that facial asymmetry below 2 mm cannot be noticed by visual assessment

Table 1
Mean and standard deviation (SD), Student's *t*-test 95% confidence interval (95 CI), P-value (P) for comparison of the means between intrauser and interuser values, and P value for the hypothesis of an absolute true difference in mean < 1 mm (P1) (Values in mm).

			Mean	SD	95 CI	P	P1
Target 1	Perimeter	Intrauser	412.2	0.9	411.9–412.6	0.11	0.59
		Interuser	413.1	2.4	412–414.1		
	Longitudinal distance	Intrauser	151.7	0.4	151.5–151.9	0.06	0.97
		Interuser	152.2	1.2	151.7–152.7		
	Transversal distance	Intrauser	104.3	0.5	104–104.5	0.17	0.99
		Interuser	104.6	0.9	104.2–104.9		
Target 2	Perimeter	Intrauser	377.8	1.5	377.1–378.4	0.4	0.85
		Interuser	378.2	2.1	377.3–379.1		
	Longitudinal distance	Intrauser	127.3	0.6	127–127.5	0.62	1
		Interuser	127.4	1.1	126.9–127.9		
	Transversal distance	Intrauser	110.9	0.5	110.7–111.1	0.38	1
		Interuser	111.0	0.7	110.8–111.3		
Target 3	Perimeter	Intrauser	430.1	1.0	429.6–430.5	< 0.001	0.03
		Interuser	432.0	2.1	431.1–432.9		
	Longitudinal distance	Intrauser	151.6	0.8	151.2–151.9	< 0.001	0.21
		Interuser	152.8	1.0	152.4–153.2		
	Transversal distance	Intrauser	117.2	0.6	117–117.5	0.019	1
		Interuser	117.7	0.6	117.4–117.9		
Target 4	Perimeter	Intrauser	367.9	1.4	367.3–368.5	0.024	0.36
		Interuser	369.1	2.0	368.2–370		
	Longitudinal distance	Intrauser	126.9	0.6	126.6–127.1	0.099	1
		Interuser	127.2	0.9	126.8–127.6		
	Transversal distance	Intrauser	111.2	0.4	111–111.3	0.062	1
		Interuser	111.6	1.0	111.2–112		
Target 5	Perimeter	Intrauser	451.3	2.2	450.4–452.2	0.002	0.05
		Interuser	453.3	2.1	452.4–454.2		
	Longitudinal distance	Intrauser	160.1	0.7	159.8–160.4	< 0.001	0.42
		Interuser	161.2	1.0	160.7–161.6		
	Transversal distance	Intrauser	122.7	1.0	122.3–123.2	0.125	0.96
		Interuser	123.2	1.0	122.8–123.6		

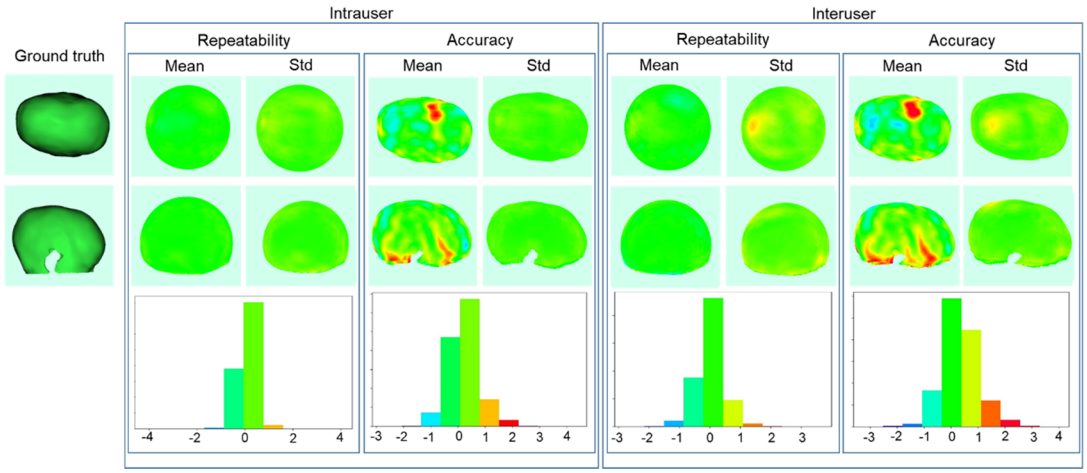

Fig. 12. Representation of distances for Target 1. For the repeatability tests, the distances are shown on a reference sphere with its centre in the model centroid. For the accuracy tests, the distances are shown on the ground truth model. Histograms for each test are shown at the bottom (values in mm).

(Pereira Silva et al., 2015). Therefore, the data provided by the PhotoMeDAS tool is enough to assess esthetical outcomes for infant's heads.

Significant differences were obtained for intrauser and interuser tests according to Student's *t* test. However, the differences in means were always below 1 mm for a 95% confidence interval. As a consequence, we can conclude that the accuracy of the smartphone-based photogrammetric solution is not greatly affected by different non-expert users.

The distribution of the error areas is especially important. Distances above 1 mm were registered in the repeatability tests in the edge of the 3D models. In these areas, the models are not as accurate due to the geometry of the image acquisition. However, the areas of inaccuracy are small enough to be ignored for deformation assessment.

Comparing the deliverables from PhotoMeDAS with the ground truth 3D models (five targets), a general overestimation is appreciated. One particular issue can be found in convex areas where higher differences (distances, cf. Fig. 7) can be achieved (e.g. Target 1). This error is given by the impossibility to assure that the cap is stuck to the infant's skin in these areas (Fig. 12).

Previous tests were carried out by the authors using a manual approach for the creation of the 3D models (Barbero-García et al., 2018). The results of the study show that the accuracy of the automatic tool is very similar to the manual approach carried out by photogrammetric experts to create the 3D models.

The difference between repeatability and accuracy tests results shows that the highest differences are given by the impossibility to properly fit the cap to the convex areas. However, these convex areas usually represent a small area of the head and do not compromise the evaluation of the general infant's head shape.

The tool provides 3D models generated from a total of 536 points, which are later interpolated to create a model. According to the results, this quantity of points can be considered enough for accurate infant's head shape representation.

4.3. Automatically-derived anthropometric linear magnitudes

The automatic anthropometric linear magnitudes show acceptable accuracy for the maximum longitudinal and transversal distances with standard deviation up to 1.17 mm. For the perimeter measurements, standard deviations rise above 2 mm in some cases. For the perimeter measurements and even for longitudinal and transversal distances in some cases, the registered accuracy is worse than the accuracy of the models. Three main reasons have been identified as possible causes of the limited accuracy of the anthropometric linear magnitudes.

(1) Firstly, the level of accuracy of the photogrammetric model is an important source of error. The correlation between the accuracy of the photogrammetric models and the accuracy of the measurements (as a difference with the average) was calculated for each model and for the automatic anthropometric linear magnitudes. For every case the correlation was negligible. The correlation was also calculated for the intrauser models only with very similar results. The lack of correlation implies that, although it can be important, the quality of the photogrammetric models is not the main factor affecting the accuracy of the automatically derived anthropometric linear magnitudes.

(2) The second source of error considered is the variability in the placement of the cap. This explains the significant differences between interuser and intrauser tests for the perimeter values according to the Student's *t*-test. A single user is supposed to have much lower variability in the process of cap and sticker placement. Differences in the placement of the cap greatly affect the obtainment of the measurements, in some cases, important differences were detected when the cap was not covering the whole forehead of the patient (Fig. 13).

(3) Lastly, the registration of the model, based on the placement of the coded stickers has an implied variability. This can result in slightly different measurements even for the same model. It could also be explaining the differences (below 1 mm for longitudinal and transversal distances but above that, in some cases, for the perimeter) between interuser and intrauser tests. The correct automatic registration of the models is a common challenge to many other methodologies used for cranial deformation analysis (De Jong et al., 2015).

Correct placement of the cap and stickers is vital for the tool to

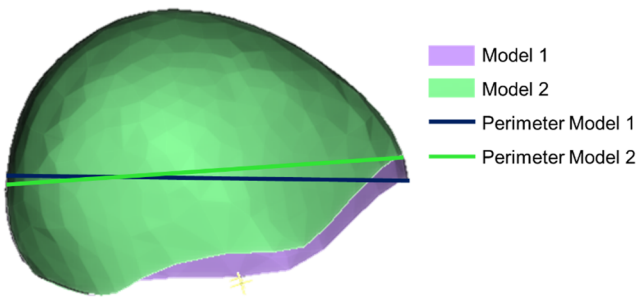

Fig. 13. Comparison of perimeter measurements between two models of the same Target.

provide useful data. However, the 3D model, together with the measurement points, are made available to the doctor in a short time frame after the data acquisition. Therefore, an error in the obtainment of the derived anthropometric linear magnitudes caused by misplacement of the cap or the stickers, could be easily noted by the doctor, who could discard the measurement and repeat the data acquisition (if required).

4.4. Comparison with current solutions

The results provide higher accuracy than to those obtained with measuring tape and calliper (Mortenson and Steinbok, 2006), especially for transversal and longitudinal distances. Moreover, the interuser reliability of the photogrammetric 3D models seems to be higher for this tool and the models provide much more complete information, as the whole infant's head is measured.

The CT and MRI, considered the gold standards, provide the highest accuracy. However, its use tends to be limited as they are costly and, more importantly, often required sedation and even imply radiation. Moreover, the lying position of the infants during radiologic image acquisition is not ideal for the assessment of the esthetical outcome of the patients.

The methodology is comparable in accuracy to low-cost scanners that are used on static targets only, such as Vectra H1 system (Canfield Imaging, NJ, USA) (Camison et al., 2018). It provides also a much more complete information than other low-cost techniques that rely in a small number of images (Lopes Alho et al., 2019).

Last but not least, high-end image-based and range-based solutions including several cameras and scanners provide higher accuracy than the presented tool (Aldridge et al., 2005; Lübbers et al., 2010). However, its present use is limited to a few clinics due to the high related cost (not only in the metrical device but maintenance, personnel, etc.). Moreover, for the particular application of cranial deformation assessment, submillimeter accuracy presents little or meaningless advantage.

5. Conclusion

The presented photogrammetric solution has been proved to be valuable for the automatic achievement of infants' head 3D models. As during a normal medical consultation, unpredicted quick infant's movements exist and it is unrealistic to carry out comprehensive intrauser and interuser tests. The analysis has been undertaken with five true 3D printed infant's head targets to assess the implemented methodology adopted in PhotoMeDAS.

The obtained accuracy is higher to commonly used methodologies such as calliper and measuring tape but it provides more complete information. Due to is low-cost, ease of use and reduced processing time, it is expected to be integrated as part of the clinical routine. Contrary to high-cost image-based and range-based devices, the PhotoMeDAS implementation can be available at primary care consultations, allowing a higher percentage of infants to be objectively tested at early stages, contributing to better outcomes and diagnosis. PhotoMeDAS can improve the assessment of an important problem such as infant's cranial deformation, without following the highly subjective manual measurements with callipers, and avoiding radiologic imaging.

In the near future, PhotoMeDAS will be clinically validated from a medical point of view on real infant's heads to assure whether it can be considered a medical device or not. Future developments will include the automatic extraction of cranial indexes as well and the improvement in the registration of the infant's head 3D models, as this has been identified in this study to be one of the major sources of metric differences.

Declaration of Competing Interest

The authors declare that they have no known competing financial interests or personal relationships that could have appeared to influence the work reported in this paper.

Acknowledgements

This project is funded by Instituto de Salud Carlos III and European Regional Development Fund (FEDER), project number PI18/00881, and by Generalitat Valenciana, grant number ACIF/2017/056.

References

Aldridge, K., Boyadjiev, S.A., Capone, G.T., DeLeon, V.B., Richtsmeier, J.T., 2005. Precision and error of three-dimensional phenotypic measures acquired from 3dMD photogrammetric images. Am. J. Med. Genet. 138 A, 247–253. https://doi.org/10.1002/ajmg.a.30959.

Argenta, L., 2004. Clinical classification of positional plagiocephaly. J. Craniofac. Surg. 15, 368–372. https://doi.org/10.1097/00001665-200405000-00004.

Ballardini, E., Sisti, M., Basaglia, N., Benedetto, M., Baldan, A., Borgna-Pignatti, C., Garani, G., 2018. Prevalence and characteristics of positional plagiocephaly in healthy full-term infants at 8–12 weeks of life. Eur. J. Pediatr. 177, 1547–1554. https://doi.org/10.1007/s00431-018-3212-0.

Barbero-García, I., Cabrelles, M., Lerma, J.L., Marqués-Mateu, Á., 2018. Smartphone-based close-range photogrammetric assessment of spherical objects. Photogramm. Rec. 33, 283–299. https://doi.org/10.1111/phor.12243.

Barbero-García, I., Lerma, J.L., Marqués-Mateu, Á., Miranda, P., 2017. Low-cost smartphone-based photogrammetry for the analysis of cranial deformation in infants. World Neurosurg. 102, 545–554. https://doi.org/10.1016/j.wneu.2017.03.015.

Barbero-García, I., Lerma, J.L., Miranda, P., Marqués-Mateu, Á., 2019. Smartphone-based photogrammetric 3D modelling assessment by comparison with radiological medical imaging for cranial deformation analysis. Measurement 131, 372–379. https://doi.org/10.1016/j.measurement.2018.08.059.

Bay, H., Ess, A., Tuytelaars, T., Gool, L. Van, 2007. Speeded-Up Robust Features (SURF). https://doi.org/10.1016/j.cviu.2007.09.014.

Bernardini, F., Mittleman, J., Rushmeier, H., Silva, C., Taubin, G., 1999. The ball-pivoting algorithm for surface reconstruction. IEEE Trans. Vis. Comput. Graph. 5, 349–359. https://doi.org/10.1109/2945.817351.

Besl, P.J., McKay, N.D., 1992. Method for registation of 3-D shapes. In: Schenker, P.S. (Ed.), Sensor Fusion IV: Control Paradigms and Data Structures. SPIE, pp. 586–606. https://doi.org/10.1117/12.57955.

Camison, L., Bykowski, M., Lee, W.W., Carlson, J.C., Roosenboom, J., Goldstein, J.A., Losee, J.E., Weinberg, S.M., 2018. Validation of the Vectra H1 portable three-dimensional photogrammetry system for facial imaging. Int. J. Oral Maxillofac. Surg. 47, 403–410. https://doi.org/10.1016/j.ijom.2017.08.008.

Caple, J.M., Stephan, C.N., Gregory, L.S., MacGregor, D.M., 2016. Effect of head position on facial soft tissue depth measurements obtained using computed tomography. J. Forensic Sci. 61, 147–152. https://doi.org/10.1111/1556-4029.12896.

Cignoni, P., Callieri, M., Corsini, M., Dellepiane, M., Ganovelli, F., Ranzuglia, G., 2008. MeshLab: an Open-Source Mesh Processing Tool. In: Scarano, V., Chiara, R. De, Erra, U. (Eds.), Eurographics Italian Chapter Conference. The Eurographics Association. https://doi.org/10.2312/LocalChapterEvents/ItalChap/ItalianChapConf2008/129-136.

Collett, B.R., Wallace, E.R., Kartin, D., Cunningham, M.L., Speltz, M.L., 2019. Cognitive outcomes and positional plagiocephaly. Pediatrics 143, e20182373. https://doi.org/10.1542/peds.2018-2373.

Da Silva, S.L.A., Tommaselli, A.M.G., Artero, A.O., 2014. Utilização de alvos codificados do tipo ARUCO na automação do processo de calibração de câmaras. Bol. Ciencias Geod. 20, 636–656. https://doi.org/10.1590/S1982-21702014000300036.

de Jong, G., Tolhuisen, M., Meulstee, J., van der Heijden, F., van Lindert, E., Borstlap, W., Maal, T., Delye, H., 2017. Radiation-free 3D head shape and volume evaluation after endoscopically assisted strip craniectomy followed by helmet therapy for trigonocephaly. J. Cranio-Maxillofacial Surg. 45, 661–671. https://doi.org/10.1016/j.jcms.2017.02.007.

De Jong, G.A., Maal, T.J.J., Delye, H., 2015. The computed cranial focal point. J. Cranio-Maxillofacial Surg. 43, 1737–1742. https://doi.org/10.1016/j.jcms.2015.08.023.

Dörhage, K.W.W., Wiltfang, J., von Grabe, V., Sonntag, A., Becker, S.T., Beck-Broichsitter, B.E., 2018. Effect of head orthoses on skull deformities in positional plagiocephaly: Evaluation of a 3-dimensional approach. J. Cranio-Maxillofacial Surg. https://doi.org/10.1016/j.jcms.2018.03.013.

Farkas, L.G., 1994. Anthropometry of the Head and Face. Raven Pr.

Garrido-Jurado, S., Muñoz-Salinas, R., Madrid-Cuevas, F.J., Medina-Carnicer, R., 2016. Generation of fiducial marker dictionaries using mixed integer linear programming. Pattern Recognit. 51, 481–491. https://doi.org/10.1016/j.patcog.2015.09.023.

Goebbels, S., Pohle-Fröhlich, R., Pricken, P., 2019. Iterative closest point algorithm for accurate registration of coarsely registered point clouds with CityGML models. In: ISPRS Annals of the Photogrammetry, Remote Sensing and Spatial Information Sciences. pp. 201–208. https://doi.org/10.5194/isprs-annals-IV-2-W5-201-2019.

Grazioso, S., Selvaggio, M., Caporaso, T., Di Gironimo, G., 2019. A digital photogrammetric method to enhance the fabrication of custom-made spinal orthoses. J. Prosthetics Orthot. 31, 133–139. https://doi.org/10.1097/JPO.0000000000000244.

Heymsfield, S.B., Bourgeois, B., Ng, B.K., Sommer, M.J., Li, X., Shepherd, J.A., 2018. Digital anthropometry: A critical review. In: European Journal of Clinical Nutrition. Nature Publishing Group, pp. 680–687. https://doi.org/10.1038/s41430-018-

0145-7.
Hsu, C.K., Hallac, R.R., Denadai, R., Wang, S.W., Kane, A.A., Lo, L.J., Chou, P.Y., 2019. Quantifying normal head form and craniofacial asymmetry of elementary school students in Taiwan. J. Plast. Reconstr. Aesthetic Surg. 72, 2033–2040. https://doi.org/10.1016/j.bjps.2019.09.005.
Jodeh, D.S., Curtis, H., Cray, J.J., Ford, J., Decker, S., Rottgers, S.A., 2018. Anthropometric evaluation of periorbital region and facial projection using three-dimensional photogrammetry. J. Craniofac. Surg. 29, 2017–2020. https://doi.org/10.1097/SCS.0000000000004761.
Kattwinkel, J., Brooks, J.G., Keenan, M.E., Malloy, M., Willinger, M., Scheers, N.J., 2000. Changing concepts of sudden infant death syndrome: Implications for infant sleeping environment and sleep position. Pediatrics. https://doi.org/10.1542/peds.105.3.650.
Khormi, Y., Chiu, M., Goodluck Tyndall, R., Mortenson, P., Smith, D., Steinbok, P., 2020. Safety and efficacy of independent allied healthcare professionals in the assessment and management of plagiocephaly patients. Child's Nerv. Syst. 36, 373–377. https://doi.org/10.1007/s00381-019-04400-z.
Kournoutas, I., Vigo, V., Chae, R., Wang, M., Gurrola, J., Abla, A.A., El-Sayed, I., Rubio, R.R., 2019. Acquisition of volumetric models of skull base anatomy using endoscopic endonasal approaches: 3D scanning of deep corridors via photogrammetry. World Neurosurg. 129, 372–377. https://doi.org/10.1016/j.wneu.2019.05.251.
Lopes Alho, E.J., Rondinoni, C., Furokawa, F.O., Monaco, B.A., 2019. Computer-assisted craniometric evaluation for diagnosis and follow-up of craniofacial asymmetries: SymMetric v. 1.0. Child's Nerv. Syst. 1–7. https://doi.org/10.1007/s00381-019-04451-2.
Lowe, D.G., 1999. Object recognition from local scale-invariant features. In: Proceedings of the International Conference on Computer Vision-Volume 2 - Volume 2, ICCV '99. IEEE Computer Society, Washington, DC, USA, p. 1150.
Lübbers, H.-T., Medinger, L., Kruse, A., Grätz, K.W., Matthews, F., 2010. Precision and accuracy of the 3dMD photogrammetric system in craniomaxillofacial application. J. Craniofac. Surg. 21, 763–767. https://doi.org/10.1097/SCS.0b013e3181d841f7.
Martiniuk, A.L.C., Vujovich-Dunn, C., Park, M., Yu, W., Lucas, B.R., 2017. Plagiocephaly and developmental delay: a systematic review. J. Dev. Behav. Pediatr. https://doi.org/10.1097/DBP.0000000000000376.
Meulstee, J.W., Verhamme, L.M., Borstlap, W.A., Van der Heijden, F., De Jong, G.A., Xi, T., Bergé, S.J., Delye, H., Maal, T.J.J., 2017. A new method for three-dimensional evaluation of the cranial shape and the automatic identification of craniosynostosis using 3D stereophotogrammetry. Int. J. Oral Maxillofac. Surg. 46, 819–826. https://doi.org/10.1016/j.ijom.2017.03.017.
Mitchell, H.L., Newton, I., 2002. Medical photogrammetric measurement: Overview and prospects. ISPRS J. Photogramm. Remote Sens. 56, 286–294. https://doi.org/10.1016/S0924-2716(02)00065-5.
Mortenson, P.A., Steinbok, P., 2006. Quantifying positional plagiocephaly: Reliability and validity of anthropometric measurements. J. Craniofac. Surg. 17, 413–419. https://doi.org/10.1097/00001665-200605000-00005.
Munn, L., Stephan, C.N., 2018. Changes in face topography from supine-to-upright position—And soft tissue correction values for craniofacial identification. Forensic Sci. Int. 289, 40–50. https://doi.org/10.1016/j.forsciint.2018.05.016.
Muñoz-Salinas, R., Marín-Jimenez, M.J., Yeguas-Bolivar, E., Medina-Carnicer, R., 2018. Mapping and Localization from Planar Markers. Pattern Recognit. 73, 158–171. https://doi.org/10.1016/j.patcog.2017.08.010.
Nahles, S., Klein, M., Yacoub, A., Neyer, J., 2018. Evaluation of positional plagiocephaly: Conventional anthropometric measurement versus laser scanning method. J. Cranio-Maxillofacial Surg. 46, 11–21. https://doi.org/10.1016/j.jcms.2017.10.010.
Nocerino, E., Poiesi, F., Locher, A., Tefera, Y.T., Remondino, F., Chippendale, P., Van Gool, L., 2017. 3D Reconstruction with a Collaborative Approach Based on Smartphones and a Cloud-based Server. ISPRS - Int. Arch. Photogramm. Remote Sens. Spat. Inf. Sci. XLII-2/W8, 187–194. https://doi.org/10.5194/isprs-archives-XLII-2-W8-187-2017.
Patias, P., 2002. Medical imaging challenges photogrammetry. ISPRS J. Photogramm. Remote Sens. 56, 295–310. https://doi.org/10.1016/S0924-2716(02)00066-7.
Peitsch, W.K., Keefer, C.H., LaBrie, R.A., Mulliken, J.B., 2004. Incidence of cranial asymmetry in healthy newborns. e72–e72. Pediatrics 110. https://doi.org/10.1542/peds.110.6.e72.
Pereira Silva, B., Jiménez-Castellanos, E., Martinez-de-Fuentes, R., Vilches Fernandez, A.A., Chu, S., 2015. Perception of maxillary dental midline shift in asymmetric faces. Int. J. Esthet. Dent. 10, 588–596.
Pierrot Deseilligny, M., Clery, I., 2012. Apero, an open source bundle adjusment software for automatic calibration and orientation of set of images. ISPRS - Int. Arch. Photogramm. Remote Sens. Spat. Inf. Sci. XXXVIII-5/, 269–276. https://doi.org/10.5194/isprsarchives-XXXVIII-5-W16-269-2011.
Romero-Ramirez, F.J., Muñoz-Salinas, R., Medina-Carnicer, R., 2018. Speeded up detection of squared fiducial markers. Image Vis. Comput. 76, 38–47. https://doi.org/10.1016/J.IMAVIS.2018.05.004.
Siegenthaler, M.H., 2015. Methods to diagnose, classify, and monitor infantile deformational plagiocephaly and brachycephaly: a narrative review. J. Chiropr. Med. 14, 191–204. https://doi.org/10.1016/j.jcm.2015.05.003.
Sirazitdinova, E., Deserno, T.M., 2017. System Design for 3D Wound Imaging Using Low-Cost Mobile Devices. In: Cook, T.S., Zhang, J. (Eds.), Proc. SPIE 10138, Medical Imaging 2017: Imaging Informatics for Healthcare, Research, and Applications. International Society for Optics and Photonics. https://doi.org/10.3233/978-1-61499-830-3-1237.
Urbanová, P., Hejna, P., Jurda, M., 2015. Testing photogrammetry-based techniques for three-dimensional surface documentation in forensic pathology. Forensic Sci. Int. 250, 77–86. https://doi.org/10.1016/j.forsciint.2015.03.005.
Ursitti, F., Fadda, T., Papetti, L., Pagnoni, M., Nicita, F., Iannetti, G., Spalice, A., 2011. Evaluation and management of nonsyndromic craniosynostosis. Acta Paediatr. 100, 1185–1194. https://doi.org/10.1111/j.1651-2227.2011.02299.x.
Wang, C., Zhang, Y., Zhou, X., 2018. Robust Image Watermarking Algorithm Based on ASIFT against Geometric Attacks. Appl. Sci. 8, 410. https://doi.org/10.3390/app8030410.
Wilbrand, J.F., Wilbrand, M., Pons-Kuehnemann, J., Blecher, J.C., Christophis, P., Howaldt, H.P., Schaaf, H., 2011. Value and reliability of anthropometric measurements of cranial deformity in early childhood. J. Cranio-Maxillofacial Surg. 39, 24–29. https://doi.org/10.1016/j.jcms.2010.03.010.
Wong, J.Y., Oh, A.K., Ohta, E., Hunt, A.T., Rogers, G.F., Mulliken, J.B., Deutsch, C.K., 2008. Validity and reliability of craniofacial anthropometric measurement of 3D digital photogrammetric images. Cleft Palate-Craniofacial J. 45, 232–239. https://doi.org/10.1597/06-175.